





RESEARCH ARTICLE | DECEMBER 19 2023

## NbN thin films grown on silicon by molecular beam epitaxy for superconducting detectors **FREE**

A. Iovan ; A. Pedeches ; T. Descamps ; H. Rotella ; I. Florea ; F. Semond; V. Zwiller  



*Appl. Phys. Lett.* 123, 252602 (2023)

<https://doi.org/10.1063/5.0175699>

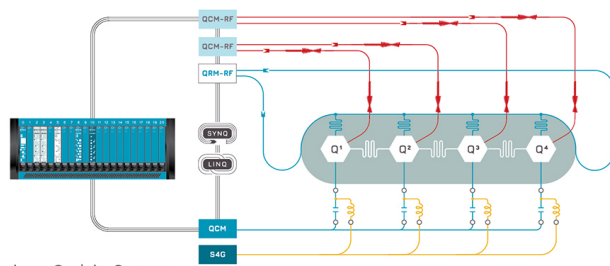


CrossMark



Integrates all Instrumentation + Software for Control and Readout of

**Superconducting Qubits**  
**NV-Centers**  
**Spin Qubits**



Superconducting Qubit Setup

[find out more >](#)

# NbN thin films grown on silicon by molecular beam epitaxy for superconducting detectors

Cite as: Appl. Phys. Lett. **123**, 252602 (2023); doi: [10.1063/5.0175699](https://doi.org/10.1063/5.0175699)

Submitted: 8 September 2023 · Accepted: 8 November 2023 ·

Published Online: 19 December 2023



View Online



Export Citation



CrossMark

A. Iovan,<sup>1</sup>  A. Pedeches,<sup>2</sup>  T. Descamps,<sup>1</sup>  H. Rotella,<sup>2</sup>  I. Florea,<sup>2</sup>  F. Semond,<sup>2</sup> and V. Zwiller<sup>1,3,a)</sup> 

## AFFILIATIONS

<sup>1</sup>Department of Applied Physics, Royal Institute of Technology, Albanova University Centre, Roslagstullsbacken 21, 106 91 Stockholm, Sweden

<sup>2</sup>Université Côte d'Azur, CNRS, CRHEA, Sophia Antipolis, France

<sup>3</sup>Single Quantum BV, Rotterdamseweg 394, 2629HH Delft, The Netherlands

<sup>a)</sup> Author to whom correspondence should be addressed: [zwiller@kth.se](mailto:zwiller@kth.se)

## ABSTRACT

Superconducting nanowire single photon detectors (SNSPDs) made with thin NbN films can reach high performances. While sputtering has been the deposition method of choice, here, we show that ammonia-molecular beam epitaxy (NH<sub>3</sub>-MBE) can produce pertinent epitaxial cubic NbN thin films on silicon substrates using an AlN buffer. Despite granular morphology and a high density of grain boundaries as well as the presence of rotational twins,  $T_c = 12.7$  K for a 5.6 nm thick film and saturation of internal detection efficiency up to 850 nm are achieved. Morphology and stoichiometry as well as strain have a strong impact on the detector properties, highlighting the importance of a precise control of the growth parameters. These results pave the way for high fabrication yield of SNSPDs on large-scale silicon wafers using epitaxial NbN thin films grown by MBE.

Published under an exclusive license by AIP Publishing. <https://doi.org/10.1063/5.0175699>

Superconducting nanowire single photon detectors (SNSPDs)<sup>1,2</sup> are widely used in a large number of applications in quantum optics.<sup>3</sup> The importance of these devices is based on their outstanding single photon detection efficiency<sup>4</sup> over an unprecedented energy range<sup>5–7</sup> combined with very high time resolution,<sup>8</sup> high saturation rates,<sup>9</sup> and very low noise.<sup>10,11</sup> These characteristics can be influenced by the choice of superconductor (NbN,<sup>12,13</sup> NbTiN,<sup>14</sup> WSi,<sup>7,15</sup> MoSi,<sup>16</sup> or high  $T_c$  material<sup>17</sup>) morphology,<sup>14</sup> thickness,<sup>18,19</sup> width,<sup>20–22</sup> photonic environment,<sup>10,23</sup> and geometrical design.<sup>24–26</sup> Scaling up this technology<sup>27</sup> to reliably produce large detectors or arrays of detectors requires films with very uniform and well-controlled properties. The most efficient superconducting nanowire single photon detectors (SNSPDs) reported till date were made with sputtered thin films, a technology compatible with silicon CMOS processes, making mass production of these detectors feasible.<sup>4</sup> However, detector fabrication yield is still an issue as pointed out in Ref. 28. Furthermore, different detection mechanisms have been proposed such as hot-spots<sup>29,30</sup> and vortices,<sup>31–34</sup> but the precise mechanism is not yet fully understood, hampering further optimization. Since materials and devices properties heavily depend on the deposition processes of the superconducting films (sputtering deposition,<sup>14</sup> atomic layer deposition,<sup>35</sup> and chemical vapor deposition<sup>36</sup>), it is pertinent to assess epitaxial NbN thin films using

molecular beam epitaxy (MBE), which allows for ultimate control of growth conditions and state of the art epitaxial heterostructures. Considering recent efforts on the epitaxy of AlN growth on silicon and the small lattice mismatch between cubic  $\delta$ -NbN and AlN, it is technologically relevant to investigate the growth of NbN on Si substrates using an AlN buffer layer for the fabrication with high yields of large areas superconducting detectors. Recently, a step was made in this direction with detectors made by MBE on AlN templates grown on sapphire was reported.<sup>28</sup> Before that, various studies<sup>27,37,38</sup> have shown the importance of the AlN template structural quality to improve the superconducting properties of detectors.

In this Letter, we demonstrate that SNSPDs can be fabricated on Si substrates using NH<sub>3</sub>-MBE, despite a high density of both cubic NbN rotational twins and threading dislocations in the AlN buffer layer. Critical temperature up to 12.7 K is measured on a 5.6 nm thick film. SNSPDs with 70 nm width showed saturation of the internal efficiency at 850 nm. We also observe that material and detection properties of thin epitaxial NbN films can be strongly modified by annealing, demonstrating the need for a fine control of overall growth conditions.

Highly resistive silicon (111) substrates are first de-oxidized *in situ* at 1200 °C, and the AlN buffer (50 nm) was grown at 1000 °C following a low temperature nucleation step at 600 °C.<sup>39</sup> For NbN

epitaxy, we explored a wide temperature range of 780–1000 °C and a wide NH<sub>3</sub>/Nb flux range, from 6 to 200 sccm corresponding to beam equivalent ratio NH<sub>3</sub>/Nb from 100 to 4000. Within these temperatures and flux ratio ranges, different NbN phases ( $\delta$ -NbN,  $\beta$ -Nb<sub>2</sub>N, and  $\epsilon$ -NbN) and/or different stoichiometries were obtained. Regardless of the phase and stoichiometry, NbN layers grown on AlN are crystalline and exhibit atomically abrupt AlN/NbN interfaces. Figure 1(a) presents a high magnification high-angle annular dark-field scanning transmission electron microscopy (HAADF)-STEM image of a 16 nm  $\delta$ -NbN layer epitaxially grown on AlN/Si. Above the crystalline NbN, an amorphous oxide layer is observed with a thickness of about 2 nm. The interface is atomically sharp [Fig. 1(b)], and the change from ABAB stacking (wurtzite AlN) to the ABC stacking from the very first monolayers indicates that the  $\delta$ -NbN cubic phase is stabilized for the chosen growth conditions (800 °C growth temperature, 6 sccm ammonia flux, and growth rate about 120 nm/h). The epitaxial relationship is as follows: NbN [111] growth axis along the AlN [0001] axis and the NbN [−110] axis along the AlN<sup>11–14,16–19</sup> axis. The presence of  $\delta$ -NbN rotational variants is visible in Fig. 1(c), where the arrows highlight the grain boundaries between domains of different crystallographic orientations. It is also visible that despite these grain boundaries, the NbN layer is continuous. X-ray diffraction analysis (XRD) (see the supplementary material) clearly shows the cubic NbN (111) diffraction peak at 35.74°. Well resolved Pendellösung fringes attest to the interfaces and the surface sharpness. All thicknesses were extracted from x-ray reflectivity analysis (XRR) and fitted with GenX software.

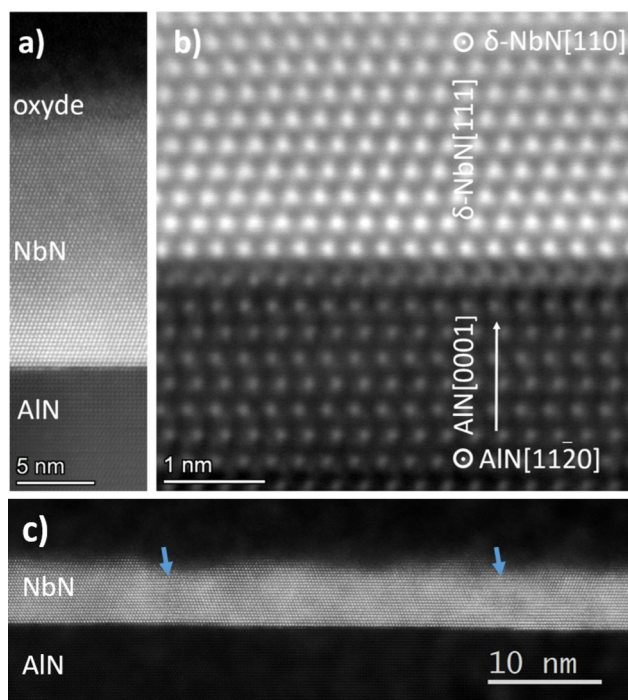


**FIG. 1.** (a) HR-HAADF STEM image of the  $\delta$ -NbN/AlN interface showing also the native NbN oxide at the surface. (b) HR-STEM image of the  $\delta$ -NbN/AlN epitaxial interface. (c) HAADF STEM image of the NbN layer showing (arrows) grains boundaries delimiting rotational variants.

For this study dedicated to the fabrication of NbN-based SNSPDs on silicon substrates, we focus on the cubic phase  $\delta$ -NbN since it is the phase with the highest critical temperature.<sup>36,40</sup> Figure 2 shows the influence of the NbN thickness on the film morphology and electrical properties. For reference, Fig. 2(a) shows an AFM image of the AlN (Al-polar) layer epitaxially grown on silicon exhibiting a smooth surface morphology (rms 1.7 Å). In addition, the AlN surface is composed of terraces with a high density of atomic steps. The streaky RHEED diagram (inset) indicates that the AlN buffer layer is monocrystalline and the growth front is two-dimensional. NbN films having different thicknesses are epitaxially grown on a 50 nm thick AlN buffer [see Fig. 2(b)]. The AFM images in Figs. 2(d) and 2(e) show that thin NbN films (5.6 and 6.9 nm) exhibit a smooth surface morphology despite the granular structure with a relatively homogeneous grain diameter distribution (around 8 nm). On the RHEED [see inset of Fig. 2(d)], the transversal offset between the spots with regard to the main streaks indicates the presence of grains having rotational twins,<sup>41</sup> as expected for the epitaxy of a cubic structure on a wurtzite structure.<sup>42</sup> Beyond a critical thickness, which depends on growth conditions, the grains coalesce to form plateaus. Figure 2(f) shows the surface morphology of such a coalesced thin film (11.5 nm thick) with grains having lateral size extending to 200 nm and separated by domain boundaries forming grooves. Coalescence is observed to occur only between grains sharing the same epitaxial relationship, leading to irregular surface patterns [Fig. 2(f)]. The progressive smoothing of the RHEED diagram allows us to follow *in situ* coalescence and expansion of domains, confirming that the granular structure tends to disappear with increasing film thickness. In Fig. 2(c), we observe that the superconducting critical temperature of cubic NbN thin films (5.6–11.5 nm) epitaxially grown on AlN on silicon is relatively high in the 11–13 K range. Interestingly, an increase in the superconducting transition temperature  $T_c$  is observed with decreasing NbN thickness. This behavior is very likely related to strain evolution as a function of NbN thickness. Tensile strain is expected from the in-plane lattice parameter mismatch between wurtzite AlN (0001) and cubic NbN (111).<sup>41</sup> The higher the tensile strain, the higher the superconducting transition temperature. Furthermore, the evaluation of the lattice parameter and deformation of the  $\delta$  NbN cubic lattice parameter, as performed in Ref. 41, indicate that the tensile strain progressively relaxes when the thickness of the NbN layer increases, which explains the decreasing  $T_c$  with thickness.

The tensile strain due to the lattice mismatch (0.48%) between  $\delta$  NbN and AlN is likely enhanced by the granular structure of NbN films.<sup>47</sup> While increasing thickness, tensile strain is first partially relaxed through elastic relaxation mechanisms and then by coalescence and formation of grooves [Fig. 2(f)]. The increase in the NbN critical temperature with increasing lattice parameter (tensile stress) up to a certain point has already been reported.<sup>41,43</sup> Since Si has a smaller thermal expansion coefficient than AlN (62% thermal expansion coefficient mismatch), AlN and then NbN thin films experience an additional tensile deformation during post-epitaxy cooling from the growth temperature to room temperature. Surprisingly, resistivity of NbN films increases with thickness, which could be related to the strain relaxation mechanism introducing defects. The correlation between the increase in  $T_c$  and the decrease in resistivity has already been observed.<sup>28,43</sup> Because MBE allows for fine tuning, correlation between resistivity and  $T_c$  as a function of thickness and strain could be carefully investigated.

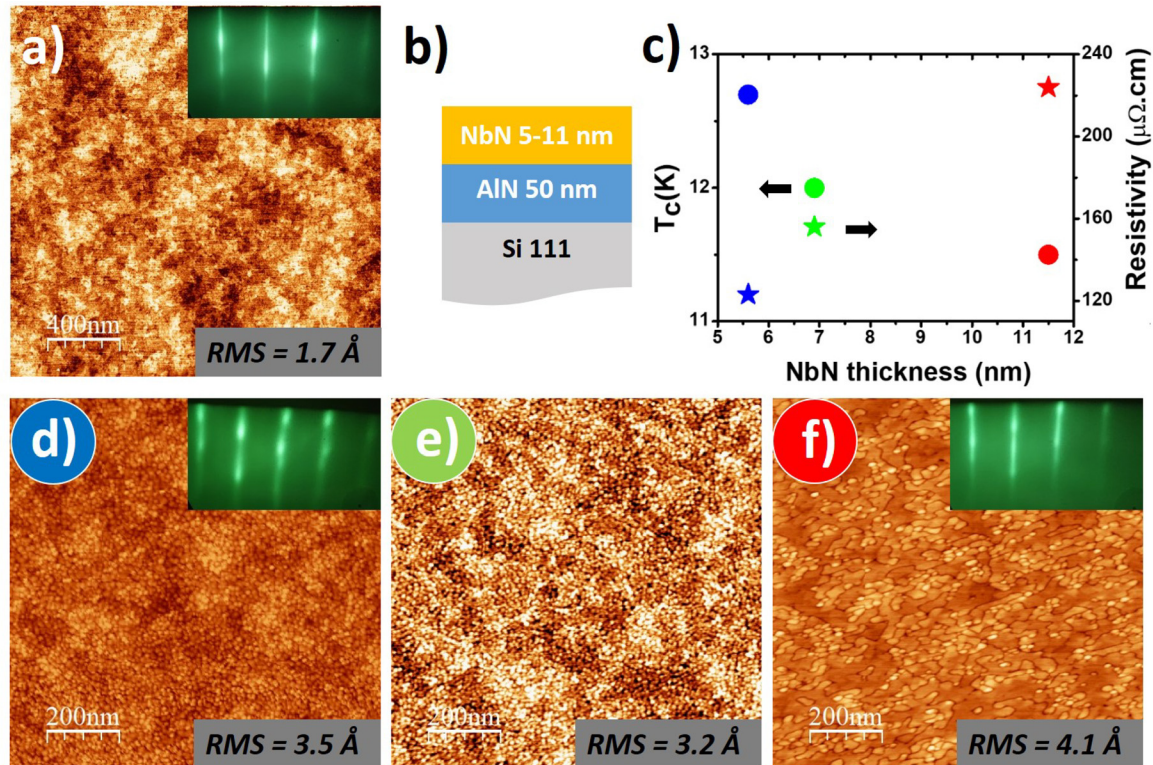


**FIG. 2.** (a) AFM picture showing the smooth surface morphology of the AlN buffer layer grown on Si. (b) Schematic representation of the samples structure presented in this paper. NbN thickness varies from 5.6 to 11.5 nm. (c) Critical temperature (circles) and resistivity (stars) of samples grown under low ammonia flux. (d)–(f) AFM pictures of NbN layers for increasing thickness under low  $\text{NH}_3$  flux. The various thicknesses are given in (c) in accordance with the color labels. Insets: RHEED patterns of the NbN layers along the [110] direction. For low thicknesses (d) and (e), a uniform grainy morphology is observed, keeping a very low roughness. Over a given critical thickness, coalescence between the grains occurs (f).

To assess the performance of these films for single photon detection, detectors were fabricated on the 6.9 nm thick film. The graph in Fig. 3(a) presents the evolution of the sheet resistance vs temperature using the four point measurements technique on patterned samples ( $25 \times 250 \mu\text{m}^2$ ). We observe a sharp transition between the normal and superconducting states and a residual resistance ratio (RRR)  $R_{300}/R_{20}$  of about 0.67. This value is similar to that obtained in a recent study.<sup>28</sup> In sputtered films, the high value of the sheet resistance is a key parameter for high quality detectors.<sup>13</sup>

Hairpin-shaped detectors with a series inductor to avoid latching were patterned with electron beam lithography (resist ma – N2401) and reactive-ion etching of NbN in a  $\text{CF}_4/\text{O}_2$  plasma. Test devices were inspected by scanning electron microscopy [Fig. 3(b)] to confirm the nanowire width uniformity over large areas and the small edge roughness. The detectors were flood illuminated at different wavelengths, and the internal detection efficiency (IDE) of 70 nm width hairpin is shown in Fig. 3(c). The detection curves were measured up to the onset of dark counts ( $29 \mu\text{A}$ ) for accurate estimation of the efficiency. Saturation of the internal detection efficiency is obtained with excitation wavelength up to 850 nm. At longer wavelengths, the efficiency drops and reaches 60% at 1550 nm based on a sigmoid curve fitting. It is important to mention that for the samples studied, the optical cavity has not been optimized and the reflection coefficient at

the AlN/NbN interface is less than 30%. A reflection of around 80% can be achieved by optimizing the cavity. These performances in terms of detection efficiency are comparable to the ones reported by Cheng *et al.*<sup>28</sup> with NbN films epitaxially grown by MBE on AlN templates on sapphire using a straight nanowire configuration. They showed saturation up to 1050 nm, at the cost of reducing the nanowire width to 20 nm and length to 20  $\mu\text{m}$ . The single photon detection pulse of our hairpin detectors for different nanowire widths is shown in Fig. 3(d). By exponential fitting of the pulse decay, the time constant decreases from 6.7 to 5 ns with increasing nanowire width from 70 to 100 nm. Assuming that the kinetic inductance of the film is much larger than the geometrical inductance of the nanowire and the series inductor, these time constants translate for a 50  $\Omega$  load impedance to a sheet kinetic inductance of the film of 58  $\text{pH}/\square$ .<sup>44</sup> Interestingly, this value is noticeably smaller than the 80  $\text{pH}/\square$  typically obtained for sputtered NbN film for a similar thickness (7 nm),<sup>45</sup> which is advantageous for experiments requiring a higher detection rate. Comparison of the results ( $T_c$  and IDE) reported in this paper and those reported in previous studies<sup>28</sup> show that it is not mandatory to achieve perfect structural quality of both the buffer layer and the NbN epitaxial layer to fabricate good detectors. This highlights that the mechanisms driving the detection processes are not well understood.

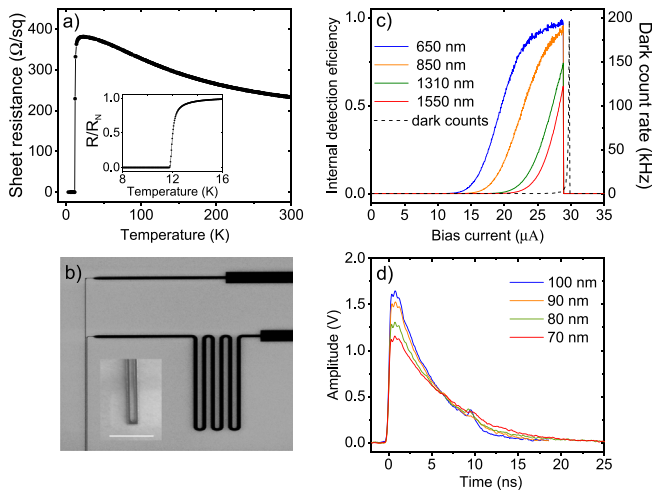


**FIG. 3.** All the data were taken with a 6.9 nm NbN film. (a) Sheet resistance vs temperature for patterned sample (the inset figure presents the measurement on the film without patterning). (b) Scanning electron microscopy (SEM) image of the hairpin detector with a series inductor (inset scale bar is 1  $\mu\text{m}$ ). (c) Internal detection efficiency for the 70 nm hairpin detector and dark counts rate. (d) Electrical pulses measured with an oscilloscope after single photon detection.

Better internal saturation at longer wavelengths is expected to occur for thinner films, since the energy required to switch the superconducting nanowire to its resistive state is reduced along with its cross section. To assess this assumption with our growth method, a thinner film (5.6 nm) was grown under the same conditions. The critical temperature remains high at 12.7 K with RRR around 0.61 [Fig. 4(a)].

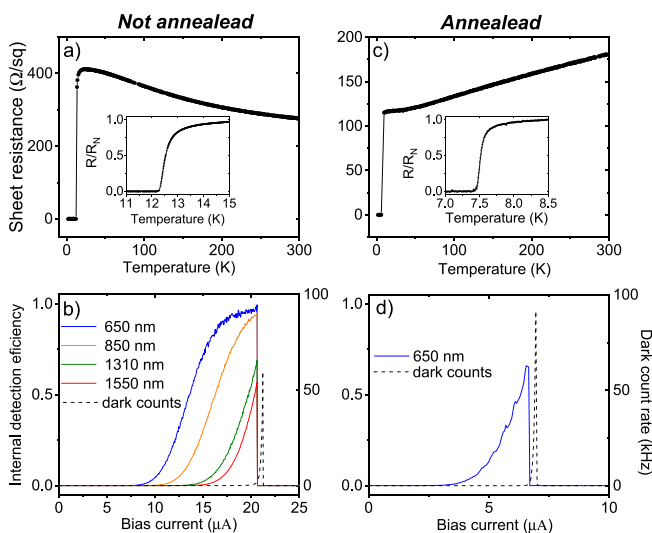


**FIG. 4.** All the measurements were performed on a 5.6 nm NbN film. (a) Sheet resistance vs temperature for patterned sample (the inset figure represents the measurement on the film without patterning). (b) Internal detection efficiency for the 70 nm hairpin nanowire and dark counts rate. (c) Sheet resistance vs temperature after *in situ* annealing on the patterned sample (the inset figure represents the measurement on the film without patterning). (d) Internal detection efficiency after *in situ* annealing for the 70 nm hairpin nanowire.

However, we obtained similar internal detection efficiency for this thinner sample, as can be seen in Fig. 4(b). The critical current for the 70 nm nanowires went from 29 to 20  $\mu\text{A}$ , but no significant improvement in the saturation current was observed at 650 and 850 nm, without any saturation at longer wavelengths. It is observed in Fig. 2 that grains tend to coalesce with the NbN thickness. To achieve a similar coalescence mechanism for a fixed thin films thickness (needed to achieve IDE saturation), annealing was performed. A cubic NbN sample having a similar thickness (5.6 nm) was grown at 800  $^{\circ}\text{C}$ , followed by an *in situ* thermal annealing at 900  $^{\circ}\text{C}$  during 3 min. To preserve the cubic phase, the annealing is carried out under an ammonia flow. As observed by AFM (shown in the supplementary material), annealing results in partially coalesced NbN layers, which is similar to what is obtained for thicker non-annealed films (Fig. 2). This change in morphology is also accompanied by a variation in refractive indices (see supplementary). This indicates that annealing is not only impacting the morphology but also the stoichiometry and/or the strain. As shown in Fig. 4(c), annealing results in a drop in the critical temperature by 5.5 K, an increase in RRR to 1.56 and also a change in the evolution of the sheet resistance slope vs temperature. The annealed sample exhibits a positive temperature coefficient of resistance until the critical temperature, which is a typical behavior for metallic films unlike the non-annealed sample exhibiting semiconductor-like temperature dependence. The quantum corrections to the temperature dependence of resistance are linked to the granularity of the films.<sup>12,46</sup> This indicates that annealing is very likely resulting in a stoichiometry modification (nitrogen depletion) or percolation of grains, which is also in agreement with the drop in the sheet resistance. In terms of the single photon detection performance, the internal efficiency clearly degraded as seen in Fig. 4(d). The critical current dropped from 21 to 7  $\mu\text{A}$ , and internal detection dropped from saturation to 65% at 650 nm. All these observations hint that a slight change in some material properties, not yet fully identified, could be responsible for a dramatic impact on the detector properties. Also, these results show that improving the surface morphology from highly dense small grains to coalesced larger grains does not necessarily improve detection performances.

In conclusion, we demonstrate that SNSPDs can be fabricated from epitaxial NbN films grown by  $\text{NH}_3$ -MBE on silicon (111) substrates using an AlN buffer layer. High critical currents and temperatures as well as saturation of the internal detection efficiency at 650 and 850 nm are shown. The fact that these good results are obtained using granular cubic NbN layers exhibiting grain boundaries and rotational twins indicates that detection mechanisms are not solely related to the crystalline quality of the superconducting layer. Nevertheless, growth parameters have to be accurately adjusted to provide performant epitaxial NbN layers for detectors. By fine-tuning these parameters for single photon applications, it is anticipated that epitaxially grown NbN by MBE on silicon substrates has the potential to outperform sputtering in terms of uniformity and reproducibility for the fabrication of low cost and large SNSPDs arrays.

See the supplementary material for XRD, ellipsometry, and AFM results on annealed and non-annealed NbN layers.

This work was supported by the French National Research Agency (ANR) under NIOBIUM convention (No. ANR-21-CE08-0037-02). We also acknowledge the support by the ANR as a part of

the “Investments for the Future” program: Labex GANEXT (Grant No. ANR-11-LABX-0014). This work was also partly supported by the Institut de Physique du CNRS (call for projects 2019). This work was partially supported by the Wallenberg Centre for Quantum Technology (WACQT) funded by Knut and Alice Wallenberg Foundation (KAW).

## AUTHOR DECLARATIONS

### Conflict of Interest

The authors have no conflicts to disclose.

### Author Contributions

A. Iovan, A. Pedeches, and T. Descamps contributed equally to this work.

**Adrian Iovan:** Investigation (equal); Methodology (equal); Writing – original draft (equal); Writing – review & editing (equal). **Antoine Pedeches:** Investigation (equal); Methodology (equal); Writing – original draft (equal); Writing – review & editing (equal). **Thomas Descamps:** Investigation (equal); Methodology (equal); Writing – original draft (equal); Writing – review & editing (equal). **Hélène Rotella:** Investigation (equal); Methodology (equal); Writing – original draft (equal); Writing – review & editing (equal). **Ileana Florea:** Investigation (equal); Methodology (equal); Writing – original draft (equal); Writing – review & editing (equal). **Fabrice Semond:** Investigation (equal); Methodology (equal); Supervision (equal); Writing – original draft (equal); Writing – review & editing (equal). **Val Zwiller:** Investigation (equal); Methodology (equal); Supervision (equal); Writing – original draft (equal); Writing – review & editing (equal).

## DATA AVAILABILITY

The data that support the findings of this study are available from the corresponding author upon reasonable request.

## REFERENCES

- G. Gol'tsman, O. Okunev, G. Chulkova, A. Lipatov, A. Semenov, B. V. K. Smirnov, A. Dzardanov, C. Williams, and R. Sobolewski, “Picosecond superconducting single-photon optical detector,” *Appl. Phys. Lett.* **79**, 705 (2001).
- R. H. Hadfield, “Single-photon detectors for optical quantum information applications,” *Nat. Photonics* **3**, 696–705 (2009).
- S. Slussarenko and G. J. Pryde, “Photonic quantum information processing: A concise review,” *Appl. Phys. Rev.* **6**, 041303 (2019).
- J. Chang, J. W. N. Los, J. O. Tenorio-Pearl, N. Noordzij, R. Gourgues, A. Guardiani, J. R. Zichi, S. F. Pereira, H. P. Urbach, V. Zwiller, S. N. Dorenbos, and I. E. Zadeh, “Detecting telecom single photons with  $99.5^{+0.5}_{-2.07}$  efficiency and high time resolution,” *APL Photonics* **6**, 036114 (2021).
- V. B. Verma, A. E. Lita, B. Korzh, E. Wollman, M. D. Shaw, R. P. Mirin, and S. W. Nam, “Towards single-photon spectroscopy in the mid-infrared using superconducting nanowire single-photon detectors,” *Proc. SPIE* **10978**, 109780N (2019).
- F. Marsili, F. Bellei, F. Najafi, A. E. Dane, E. A. Dauler, R. J. Molnar, and K. K. Berggren, “Efficient single photon detection from 500 nm to 5  $\mu$ m wavelength,” *Nano Lett.* **12**, 4799 (2012).
- V. B. Verma, B. Korzh, A. B. Walter, A. E. Lita, R. M. Briggs, M. Colangelo, Y. Zhai, E. E. Wollman, A. D. Beyer, J. P. Allmaras, H. Vora, D. Zhu, E. Schmidt, A. G. Kozorezov, K. K. Berggren, R. P. Mirin, S. W. Nam, and M. D. Shaw, “Single-photon detection in the mid-infrared up to 10  $\mu$ m wavelength using tungsten silicide superconducting nanowire detectors featured,” *APL Photonics* **6**, 056101 (2021).
- F. Marsili, V. B. Verma, J. A. Stern, S. Harrington, A. E. L. T. Gerrits, I. Vayshenker, B. Baek, M. D. Shaw, R. P. Mirin, and S. W. Nam, “Detecting single infrared photons with 93% system efficiency,” *Nat. Photonics* **7**, 210–214 (2013).
- F. Marsili, F. Najafia, E. Dauler, F. Bellei, X. Hu, M. Csete, R. J. Molnar, and K. K. Berggren, “Single-photon detectors based on ultranarrow superconducting nanowires,” *Nano Lett.* **11**, 2048 (2011).
- C. Chuck, W. H. P. Pernice, and H. X. Tang, “Waveguide integrated low noise NbTiN nanowire single-photon detectors with milli-Hz dark count rate,” *Sci. Rep.* **3**, 1893 (2013).
- H. Shibata, K. Shimizu, and H. T. Y. Tokura, “Ultimate low system dark-count rate for superconducting nanowire single-photon detector,” *Opt. Lett.* **40**, 3428 (2015).
- K. Smirnov, A. Divoichiy, Y. Vakhtomin, P. Morozov, P. Zolotov, A. Antipov, and V. Seleznev, “NbN single-photon detectors with saturated dependence of quantum efficiency,” *Supercond. Sci. Technol.* **31**, 035011 (2018).
- P. Zolotov, S. Svyatodukh, A. Divoichiy, V. Seleznev, and G. Goltsman, “High-resistivity niobium nitride films for saturated-efficiency SMSPDs at telecom wavelengths and beyond,” *Appl. Phys. Lett.* **122**, 152602 (2023).
- S. Steinhauer, L. Yang, S. Gyger, T. Lettner, C. Errando-Herranz, K. D. Jöns, M. A. B. K. Gallo, J. Zichi, and V. Zwiller, “NbTiN thin films for superconducting photon detectors on photonic and two-dimensional materials,” *Appl. Phys. Lett.* **116**, 171101 (2020).
- B. Baek, A. E. Lita, V. Verma, and S. W. Nam, “Superconducting a- $W_xSi_{1-x}$  nanowire single-photon detector with saturated internal quantum efficiency from visible to 1850 nm,” *Appl. Phys. Lett.* **98**, 251105 (2011).
- Y. P. Korneeva, M. Y. Mikhailov, Y. P. Pershin, N. Manova, A. Divoichiy, Y. B. Vakhtomin, A. Korneev, K. Smirnov, A. Sivakov, A. Y. Devizenko, and G. N. Goltsman, “Superconducting single-photon detector made of MoSi film,” *Supercond. Sci. Technol.* **27**, 095012 (2014).
- I. Charaev, D. A. Bandurin, A. T. Bollinger, I. Y. Phinney, I. Drozdov, M. Colangelo, B. A. Butters, T. Taniguchi, K. Watanabe, O. M. X. He, I. Božović, P. Jarillo-Herrero, and K. K. Berggren, “Single-photon detection using high-temperature superconductors,” *Nat. Nanotechnol.* **18**, 343–349 (2023).
- A. Lipatov, O. Okunev, K. Smirnov, G. Chulkova, A. Korneev, P. Kouminov, G. Gol'tsman, J. Zhang, W. Slys, A. Verevkin, and R. Sobolewski, “An ultrafast NbN hot-electron single-photon detector for electronic applications,” *Nano Lett.* **15**, 1689 (2015).
- M. Hofherr, D. Rall, K. Ilin, M. Siegel, A. Semenov, H.-W. Hübers, and N. A. Gippius, “Intrinsic detection efficiency of superconducting nanowire single-photon detectors with different thicknesses,” *J. Appl. Phys.* **108**, 014507 (2010).
- F. Najafi, F. Marsili, E. Dauler, R. J. Molnar, and K. K. Berggren, “Timing performance of 30-nm-wide superconducting nanowire avalanche photodetectors,” *Appl. Phys. Lett.* **100**, 152602 (2012).
- Y. Korneeva, D. Vodolazov, A. Semenov, I. Florya, N. Simonov, A. K. E. Baeva, G. Goltsman, and T. M. Klapwijk, “Optical single-photon detection in micrometer-scale NbN bridges,” *Phys. Rev. Appl.* **9**, 064037 (2018).
- M. Yabuno, F. China, S. Miki, and H. Terai, “Large-area niobium titanium nitride superconducting microstrip single-photon detector fabricated using a photolithography process,” *IEEE Trans. Appl. Supercond.* **33**, 2200104 (2023).
- L. Redaelli, G. Bulgarini, S. Dobrovolskiy, S. Dorenbos, V. Zwiller, E. Monroy, and J. M. Gérard, “Design of broadband high-efficiency superconducting-nanowire single photon detectors,” *Supercond. Sci. Technol.* **29**, 065016 (2016).
- D. Henrich, P. Reichensperger, M. Hofherr, J. M. Meckbach, K. Il'in, M. Siegel, A. Z. A. Semenov, and D. Y. Vodolazov, “Geometry-induced reduction of the critical current in superconducting nanowires,” *Phys. Rev. B* **86**, 144504 (2012).
- H. L. Hortensius, E. F. C. Driessen, T. M. Klapwijk, K. K. Berggren, and J. R. Clem, “Critical-current reduction in thin superconducting wires due to current crowding,” *Appl. Phys. Lett.* **100**, 182602 (2012).
- M. Jönsson, R. Vedin, S. Gyger, J. A. Sutton, S. Steinhauer, V. Zwiller, M. Wallin, and J. Lidmar, “Current crowding in nanoscale superconductors within the Ginzburg-Landau model,” *Phys. Rev. Appl.* **17**, 064046 (2022).
- R. Rhazi, H. Machhadani, C. Bougerol, S. Lequien, E. Robin, G. Rodriguez, R. Souil, J.-L. Thomassin, N. Mollard, Y. Désières, E. Monroy, S. Olivier, and J.-M.

- Gérard, "Improvement of critical temperature of niobium nitride deposited on 8-inch silicon wafers thanks to an AlN buffer layer," *Supercond. Sci. Technol.* **34**, 045002 (2021).
- <sup>28</sup>R. Cheng, J. Wright, H. G. Xing, D. Jena, and H. X. Tang, "Epitaxial niobium nitride superconducting nanowire single-photon detectors," *Appl. Phys. Lett.* **117**, 132601 (2020).
- <sup>29</sup>J. J. Renema, R. Gaudio, Q. Wang, Z. Zhou, A. Gaggero, F. Mattioli, R. Leoni, D. Sahin, M. J. A. de Dood, A. Fiore, and M. P. van Exter, "Experimental test of theories of the detection mechanism in a nanowire superconducting single photon detector," *Phys. Rev. Lett.* **112**, 117604 (2014).
- <sup>30</sup>A. Engel and A. Schilling, "Numerical analysis of detection-mechanism models of superconducting nanowire single-photon detector," *J. Appl. Phys.* **114**, 214501 (2013).
- <sup>31</sup>L. N. Bulaevskii, M. J. Graf, and V. G. Kogan, "Vortex-assisted photon counts and their magnetic field dependence in single-photon superconducting detectors," *Phys. Rev. B* **85**, 014505 (2012).
- <sup>32</sup>A. Engel, J. J. Renema, K. Il'in, and A. Semenov, "Detection mechanism of superconducting nanowire single-photon detectors," *Supercond. Sci. Technol.* **28**, 114003 (2015).
- <sup>33</sup>J. J. Renema, Q. Wang, R. Gaudio, I. Komen, K. op't Hoog, D. Sahin, A. Schilling, M. P. van Exter, A. Fiore, A. Engel, and M. J. A. de Dood, "Position-dependent local detection efficiency in a nanowire superconducting single-photon detector," *Nano Lett.* **15**, 4541–4545 (2015).
- <sup>34</sup>D. Y. Vodolazov, Y. P. Korneeva, A. V. Semenov, A. A. Korneev, and G. N. Goltsman, "Vortex-assisted mechanism of photon counting in a superconducting nanowire single-photon detector revealed by external magnetic field," *Phys. Rev. B* **92**, 104503 (2015).
- <sup>35</sup>R. Cheng, S. Wang, and H. X. Tang, "Superconducting nanowire single-photon detectors fabricated from atomic-layer-deposited NbN," *Appl. Phys. Lett.* **115**, 241101 (2019).
- <sup>36</sup>D. Hazra, N. Tsavdaris, and M. Mofheinz *et al.*, "Superconducting properties of very high quality NbN thin films grown by high temperature chemical vapor deposition," *Supercond. Sci. Technol.* **29**, 105011 (2016).
- <sup>37</sup>D. Sam-Giao, S. Pouget, C. Bougerol, E. Monroy, A. Grimm, S. Jebari, M. Hofheinz, J. M. Gérard, and V. Zwiller, "High-quality NbN nanofilms on a GaN/AlN heterostructure," *AIP Adv.* **4**, 107123 (2014).
- <sup>38</sup>H. Machhadani, J. Zichi, C. Bougerol, S. Lequien, J.-L. Thomassin, A. Mukhtorava, V. Zwiller, J. Gérard, and E. Monroy, "Improvement of the critical temperature of NbTiN films on III-nitride substrates," *Supercond. Sci. Technol.* **32**, 035008 (2019).
- <sup>39</sup>F. Semond, "Epitaxial challenges of GaN on silicon," *MRS Bull.* **40**, 412 (2015).
- <sup>40</sup>A. Kobayashi, S. Kihira, T. Takeda, M. Kobayashi, T. Harada, K. Ueno, and H. Fujioka, "Crystal-phase controlled epitaxial growth of NbN, superconductors on wide-bandgap AlN semiconductors," *Adv. Mater. Interfaces* **9**, 2201244 (2022).
- <sup>41</sup>A. Kobayashi, K. Ueno, and H. Fujioka, "Coherent epitaxial growth of superconducting NbN ultrathin films on AlN by sputtering," *Appl. Phys. Express* **13**, 061006 (2020).
- <sup>42</sup>M. Grundmann, "Formation of epitaxial domains: Unified theory of survey of experimental results," *Phys. Status Solidi B* **248**, 805–824 (2011).
- <sup>43</sup>Z. Wang, A. Kawakami, Y. Uzawa, and B. Komiyama, "Superconducting properties and crystal structures of single-crystal niobium nitride thin films deposited at ambient substrate temperature," *J. Appl. Phys.* **79**, 7837–7842 (1996).
- <sup>44</sup>I. Holzman and Y. Ivry, "Superconducting nanowires for single-photon detection: Progress, challenges, and opportunities," *Adv. Quantum Technol.* **116**, 1800058 (2019).
- <sup>45</sup>M. Colangelo, B. Korzh, J. Allmaras, A. Beyer, A. Mueller, R. Briggs, B. Bumble, M. Runyan, M. Stevens, A. McCaughan, D. Zhu, S. Smith, W. Becker, L. Narvaez, J. Bienfang, S. Frasca, A. Velasco, C. Pena, E. Ramirez, A. Walter, E. Schmidt, E. Wollman, M. Spiropulu, R. Mirin, S. W. Nam, K. Berggren, and M. Shaw, "Impedance-matched differential superconducting nanowire detectors," *Phys. Rev. Appl.* **19**, 044093 (2023).
- <sup>46</sup>C. Carbillet, S. Caprara, M. Grilli, C. Brun, T. Cren, F. Debontridder, B. Vignolle, W. Tabis, D. Demaille, L. Largeau, K. Ilin, M. Siegel, D. Roditchev, and B. Leridon, "Confinement of superconducting fluctuations due to emergent electronic inhomogeneities," *Phys. Rev. B* **93**, 144509 (2016).
- <sup>47</sup>W. Nix and B. Clemens, "Crystallite coalescence: A mechanism for intrinsic tensile stresses in thin films," *J. Mater. Res.* **14**, 3467–3473 (1999).